Intepretation of polarimetric radar measurements at X band for volcanic plume monitoring

Mario Montopoli

Mario Montopoli[1,2], Gianfranco Vulpiani[3], Frank Marzano[1,2], Errico Picciotti[1,4], Saverio Di Fabio[1]

[1]*CETEMPS, University of L'Aquila, Via Vetoio, 67100, L'Aquila, Italy*
[2]*Dep. of Information Engineering, Electronics and Telecommunications, Sapienza University of Rome, Rome, Italy*
[3]*Department of Civil Protection, Rome, Italy*
[4]*Himet srl, L'Aquila, Italy*

(Dated: 18 July 2014)

1 Introduction

In recent years, several works have investigated the potential role played by ground-based microwave weather radars for the monitoring of volcanic ash clouds (*Rose at al., 2000, Mastin et al., 2009, Maki et al., 2012, Vulpiani et al., 2011 and Marzano et al., 2013*). The goal of this work is to show the potentiality and drawbacks of the X-band dual polarization radar measurements (DPX) through the data acquired during the Grímsvötn (Iceland) volcanic eruptions that took place in 2011. The analysis is enriched by the comparison between X band data and the observations from the satellite Special Sensor Microwave Imager/Sounder (SSMIS) or the Icelandic eruption. X-band radars and SSMIS radiometer cover a large range of the microwave spectrum. The inter-comparison between these two sources is made in terms of total columnar concentration (*TCC*). The latter is estimated from radar observables using the "volcanic ash radar retrieval" (VARR) algorithm *(Marzano et al., 2012*) for dual-polarization X-band and single polarization C-band systems and from SSMIS brightness temperature (BT) using a linear BT–TCC relationship. VARR, in its general version, also include a detection module for distinguishing ash from meteorological targets. The ash detection would be the first step in an operational context before proceeding with its quantitative estimation. This module is based on the temporal analysis of radar volumes and geographical information, following a fuzzy logic approach. The output of the detection procedure is a Probability of Ash Detection (PAD) index from witch meteo and ash targets are discriminated. Results show that DPX radar data identify an evident volcanic signature, even though the interpretation of the polarimetric variables is not always straightforward, likely due to the possible formation of ash and ice particle aggregates and the radar signal impairments like depolarization or non-uniform beam filling that might be caused by turbulence effects. The good correlation between DPX and SSMIS is also encouraging for the use of space-based microwave sensors for aiding the more conventional infrared retrievals of ash in proximity of the erupting column.

2 Case of study

The considered case study is the volcanic eruption occurred in May 2011 at the Grímsvötn volcano, located in the northwest of the Vatnajökull glacier in south-east Iceland. It is one of Iceland's most active volcanoes. An explosive subglacial volcanic eruption started in the Grímsvötn caldera in southern Iceland around 19:00 UTC on 21st May 2011. The strength of the eruption decreased rapidly and the plume was below ~10 km altitude after 24 h. The eruption was officially declared over on 28 May at 07:00 UTC. More details on the Grímsvötn eruption can be found in *Petersen et al. (2012)*, *and Montopoli et al. (2014)* where a complete analysis of the Grímsvötn event can be found.

3 Data Description

Radar data The X-band dual polarization radar measurements (DPX) used in this study are acquired by the Meteor 50DX system which is a mobile compact weather radar deployed on a transportable trailer. For the volcanic event of May 2011 in Iceland, it has been positioned in the Kirkjubæjarklaustur, southern Iceland, at approximately 70 km away from the Grímsvötn volcano. At the time of the Grímsvötn eruption, the DPX radar was on loan to the Iceland Meteorological office under an agreement with the Italian department of civil protection. During its operational activities of May 2011, DPX scans were set to 14 elevations angles from 0.7 to 40 deg while the PRF=550 Hz, pulse duration =1.33 μs and the number of integrated pulses was 23. The DPX radar output variables that we analysed are the co-polar and differential reflectivity, the correlation coefficient and the differential phase shift, respectively indicated by Z_{HH} [dBZ], Z_{DR} [dB], ρ_{HV} [-] and K_{DP} [deg/km]. Those variables have a range, azimuth and time sampling of 0.20 km and 1 deg and 10 min, respectively. The radar variables are post-processed to include a non uniform beam filling compensation of ρ_{HV} as in (*Ryzhkov 2007*), ground clutters filtering and KDP estimation using an approach similar to *Vulpiani et al, 2012, Z_{HH}* partial beam blocks compensation as in (*Bech et al, 2003*) while efforts for the external calibration of Z_{DR} using vertical scans in low rain regimes did not provide the expected accuracy results probably due to the difficulties to intercept low rain regimes in Iceland in May 2011. For this reason Z_{DR} is left unchanged to its original output from DPX software. **Figure 1** (left panels) shows an example of range- height scans (RHI) of radar variables on May 22nd 2011, 07:12 UTC while an ash plume was developing. The right panels of the same figure shows the temporal trends of each radar variable for selected points as indicated by black crosses in the left panel.

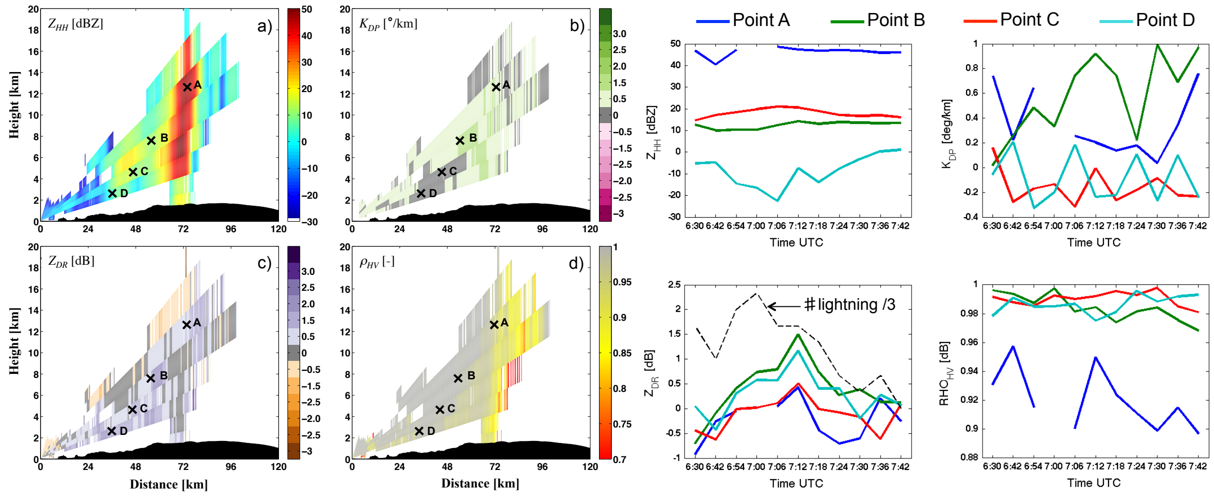

***Figure 1**: Left: RHI of radar variables as listed in the top panel text for the case study of 22nd of May 2011, 7:12 UTC, respectively. Right panels show the temporal evolution of each radar variables on the left for the black crosses on the left.*

Figure 2 shows the range profile of the radar variables shown in figure 1 along four selected elevation angles. The profile of the height of the radar ray paths is also shown by shaded line. A vertical line marks the position of the Grímsvötn caldera. Z_{HH} strongly decreases with distance with respect to its maximum although the volcanic plume signature is still evident close to the radar position (i.e. approximately 70 km far from the Grímsvötn caldera). ρ_{HV} starts decreasing when the maximum of reflectivity is reached. Non uniform beam filling (NUBF), likely due to turbulence effects, might be responsible for such a decrements of ρ_{HV} nevertheless its partial compensation. Indeed, occasionally, ρ_{HV}, starts to increase again after the plume core, for example at elevation of 6.30 deg, suggesting the strong contribution of the turbulence effects to the NUBF within the ash cloud. In that region, when Z_{HH} reaches its maximum of approximately 50 dB, ρ_{HV} starts decreasing reaching values lower as 0.7. In the range gates within the plume, K_{DP} shows positive values that occasionally go beyond 1.5 deg/km. Areas outside the core of the plume show K_{DP} close to zero or nearly negative. A positive correlation of about 0.4 has been found between K_{DP} and Z_{HH} (not shown). The behaviour of K_{DP} might suggest a different particle orientation inside and outside the plume core. The analysis of Z_{DR} tends to confirm this aspect. Although the calibration of Z_{DR} is not accurately verified and it cannot be used to make quantitative conclusions, the spatial variability of its values can still provide some information. Values of Z_{DR} nearly zero or slightly negative inside the core of the volcanic plume, are quite evident with respect to those outside. In the range distances from 10 to 60 km, the increase of Z_{DR} at the lower elevation, close to the ground, (upper left panel of figure 2) may suggest the aggregation of small ash particles coated by ice. It is worth noting that, Z_{DR} may be also corrupted by depolarization effects and differential attenuation due to the presence of ice columns that align under the effect of the atmospheric electrification (*Ryzhkov and Zrnic, 2007*). The temporal trend of lightinings registered around 07:12 UTC is shown in the right panel of figure 1. Even though several lightnings have been registered within the plume core by the world wide lightning location network we did not find a clear correlation with available radar polarimetric signature so we argue that that depolarization effects might be due also to strong turbulences within the ash column.

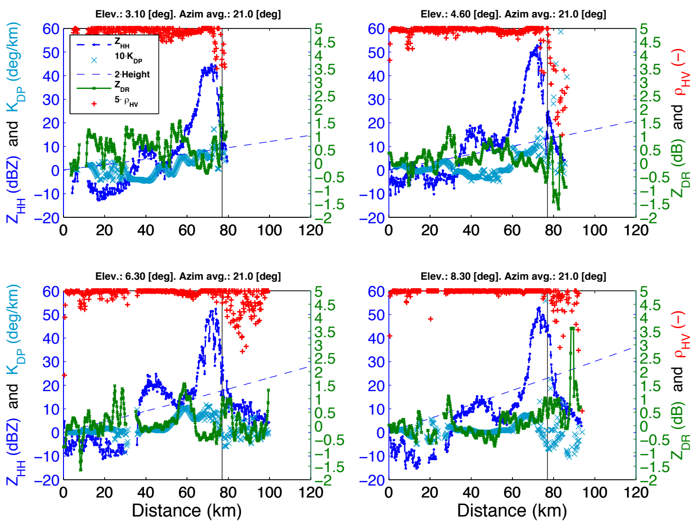

***Figure 2**: range profiles of radar variables around the direction of 21 deg considered in the RHI of figure 1. The four panels refer to different elevation angles as indicated in each title's panel.*

Radiometer data. The radiometer data used in this study come from the SSMIS sensor which flights aboard the LEO DMSP platforms orbiting at 833 km height above ground (*Kramer, 2002*). SSMIS is a conically scanning passive microwave radiometer with several channels in the 19 to 189 GHz range and a swath of approximately 1700 km. The observation angle between the nadir direction and the antenna pointing direction is 45 degrees. SSMIS measures the spectral radiances from the observed scene usually given in terms of brightness temperature (*BT*). *BT* is frequency and polarization dependent so that both horizontally-polarized BT_H and vertically-polarized BT_V can be available in principle. For the study of ash the SSMIS channels that potentially show an ash signature are those at frequencies and spatial sampling as follows (in [GHz]/[km]): [183±6]/[12.5], [183±3]/[12.5], [183±1]/[12.5], [150.0]/[12.5] and [91.6]/[12.5]. *BT* data are provided as calibrated geo-referenced data for which the antenna pattern effect is already accounted. The geolocation error is estimated as approximately 1 pixel, and thus a pointing refinement may be applied using the coastline reference. An SSMI overpass above the Grímsvötn on 22nd May 2011 at 07:15 UTC is shown in figure 3 for various frequency bands as in the panel's title. Some further descriptions of SSMIS characteristics and data processing for ash cloud observations may be also found in Montopoli et al. (2013). **Figure 3** (right panel) shows an example of horizontal profiles of brightness temperature at horizontal polarization, BTH, in [K] at frequency [GHz] of 150.0, 183±1, 183±3 and 183±6. The depression of BTH around 64.3 deg latitude, shown in all right panels and evident in the maps in the left panels, is a signature of the volcanic plume. It is probably due to the scattering of radiation along different paths than the pointing direction of 45 deg with respect the nadir. A comparison among the observed BTHs shows a stronger signature at 183±6 GHz through a larger dynamic range. For this reason, the channel at 183±6 GHz will be considered for comparison with radar estimates which are shown in the result section. Figure 3 highlights as microwave radiometers' channels above 100GHz can in principle support the ash detection of volcanic plumes close to the vent where infrared radiometers channels (usually 11 μm 12μm) might saturate giving no ash signal.

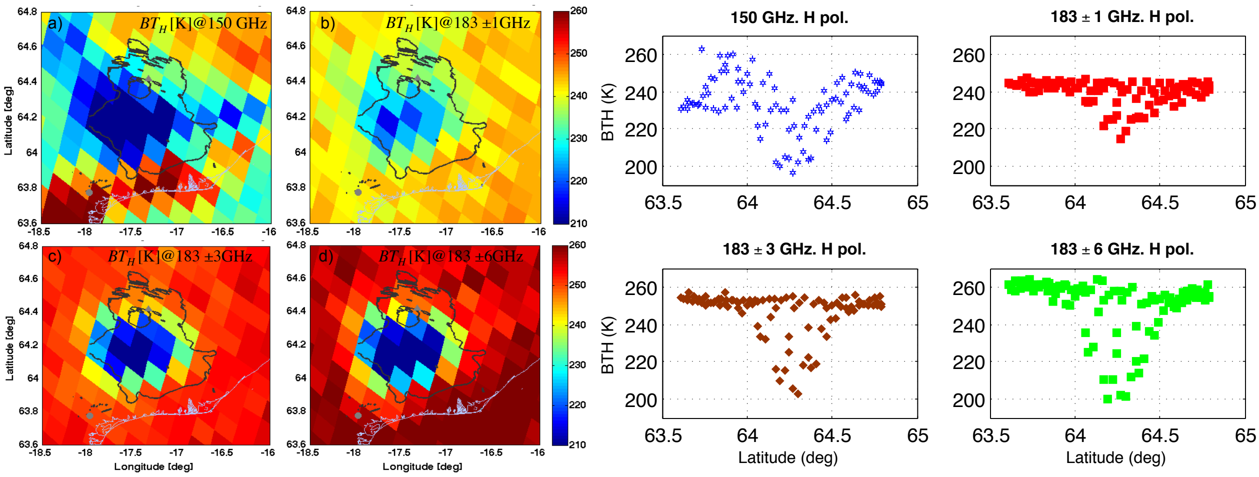

Figure 3*: Left: brightness temperature, BT_H, in [K] from SSMIS on DMSP F-17. Data were acquired at 07:15 UTC on May 22nd 2011. Contours of the radar reflectivity at 5 and 30 dBZ are shown using black lines. The radar and the Grímsvötn volcano positions are indicated with the symbols "O" and "Δ", respectively. Coastlines are indicated by bright gray lines. Right: Horizontal profiles of BTH along the Latitude direction. Right: horizontal profiles of BTH.*

4 Volcanic ash radar / radiometer retrieval (VARR)

The VARR procedure foresees two steps: ash detection and ash estimation as briefly described below.

Ash radar detection. Radar detection of ash clouds is a cumbersome problem, as their signature can be confused with that originated by hydrometeors. The ash detection methodology here described is based on the temporal analysis of radar volumes of reflectivity and geographical information for the specific area considered. The basic idea is to run a background process, which performs a special analysis on the areas surrounding the volcano vent. When the ash detection test is passed (i.e. an eruption is detected), the radar processing chain switches (manually or automatically, depending on the system) into an ash modality and classification and estimation procedure can start.

The proposed detection technique is applied to three concentric circular sectors s_1, s_2, s_3 of diameters $d_1 < d_2 < d_3$ centered on the volcano position. It works using the VMI and the ECHO-Top radar products indicated by $Z_{sk}(i,j,t_n)$), $H_{sk}(i,j,t_n)$, respectively, and the percentage of pixels of Z_{sk} above the threshold S_{zsk}, indicated by $N_{si}(i,j,t_n)$. Note that Z_{si}, H_{si}, N_{si} are quantities that are calculated for each radar time sampling "t_n" and for each horizontal pixel (i,j) within each sector "s_k".

A ramp membership function, $M(X, X_{th}, \Delta X)$, is then used to convert "X" into a membership probability with $X = Z_{si}$ or H_{si} or N_{si}. The parameters X_{th} and ΔX are so that $M(X<X_{th})=0$, $M(X>X_{th}+\Delta X)=1$, $M(X_{th} \leq X \leq X_{th}+\Delta X)=\Delta X^{-1} \bullet (X-X_{th})$ and their values depend on scan strategy, distance volcano-radar and their respective altitude, azimuth and range resolution, radar measurements and the circular sector considered. Thus, for each instant t_n, we assign a label "Y" or "N" to each sector s_k, taking the maximum of the products of the membership functions of Z, H and N in the domain s_k and checking if it is greater of lesser than 0.5:

$$\max_{sk}\left\{M(Z_{\mathrm{sk}})M(H_{\mathrm{sk}})M(N_{\mathrm{sk}})\right\}=\begin{cases}\geq 0.5 & \Rightarrow \quad s_k = Y\ (YES)\\ <0.5 & \Rightarrow \quad s_k = N\ (NO)\end{cases} \tag{1}$$

Roughly speaking eq. (1) reveals the presence of ash in the domain s_k (i.e. s_k=Y) if there is a sufficient number of pixels, if those pixel lies in a specified range of altitudes and if the reflectivity is sufficient high. The different combinations for s_k=Y or N at instant t_n and t_{n-i}, are then traduced into a Probability of Ash Detection PAD as follows.

$$PAD(t_n)=p_{ash}(t_n,s_1=Y\,|\,s_2,s_3)\left[\frac{1}{N_V}\sum_{i=1}^{N_V}p_{ash}(t_{n-i},s_1\,|\,s_2,s_3)\right] \tag{2}$$

Note that PAD in (2) is the product of two conditional probabilities of ash: the current probability of ash when in sector s_1, when s_1=Y, $p_{ash}(t_n,s_1$=Y$|s_2,s_3)$, and the temporal average of past probabilities in sector s_1: $p_{ash}(t_{n-i},s_1|s_2,s_3)$ both conditioned to the outcomes of (1) in sectors s_2 and s_3. Both $p_{ash}(t_n)$ and $p_{ash}(t_{n-i})$ are preselected probabilities as indicated in the table in **figure 4**. The time span of the average probability is set through Nv. In our case, Nv is so that it covers 1-hour. Note that, if at the current instant, t_n, s_1=N, PAD is automatically set to zero so that eq. (2) applies only when at t_n, s_1=Y. The preselected values in the table of figure 4 for p_{ash} basically guarantee that ash is not detected in cases where persistent and/or widespread radar echoes, likely due to moving stratiform storms, cover the chosen sectors in the volcano surrounding. Of course convective developing close to the volcano might be likely confused with an ash plume. In this respect polarimetry could help in refining the detection procedure. From our experience for the cases of Etna and Grimvotn volcano, PAD ≥ 0.8 are associated to the presence of ash while PAD≤ 0.6 are mainly due to meteorological factors. The detection algorithm was tested for Grimsvotn eruption case study after adapting the parameters for that site. A nice result is shown in *figure 4* where two examples at two different instant are shown, The temporal sequence of PAD, which might represent an operational warning product of VARR is shown in **figure 5**. In this figure gray areas indicates the instants where we found a plume by visual inspection of each radar scan. The marker colors in the PAD sequence refers to hit false and miss plume detection as specified in the figure legend. The hit rate (green circles on grey areas) is high and this is an encouraging results for further test.

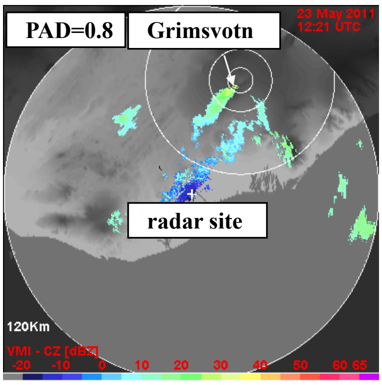

Ash conditioned probabilities
$P_{ash}(t_n,s_1$=Y $\|s_2$=Y,s_3=Y$)$=0
$P_{ash}(t_n,s_1$=Y $\|s_2$=Y,s_3=N$)$=0.50
$P_{ash}(t_n,s_1$=Y $\|s_2$=N,s_3=Y$)$=0.70
$P_{ash}(t_n,s_1$=Y $\|s_2$=N,s_3=N$)$=1
$P_{ash}(t_{n-i},s_1$= N $\|s_2$=Y,s_3=Y$)$=0
$P_{ash}(t_{n-i},s_1$= N $\|s_2$=Y,s_3=N$)$=0.75
$P_{ash}(t_{n-i},s_1$= N $\|s_2$=N,s_3=Y$)$=0.65
$P_{ash}(t_{n-i},s_1$= N $\|s_2$=N,s_3=N$)$=1

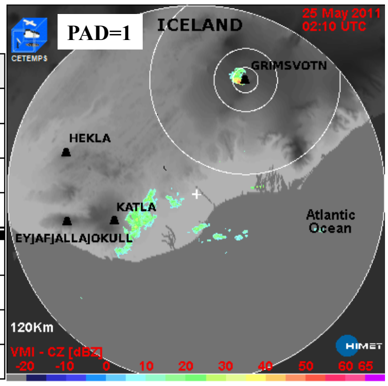

***Figure 4**. left and right: VMI radar images of Grimsvotn eruption on May 23, 2011 12:21 UTC (PAD=0.8) and May 25th , 2011, 02:10 UTC (PAD=1), respectively. PAD value computed from the beginning of the event confirming the ongoing eruption. Middle: values of p_{ash} used in (2).*

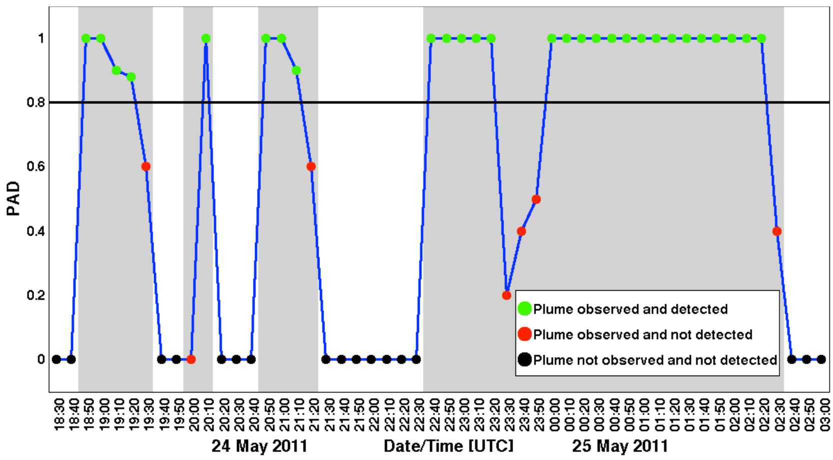

***Figure 5**. Temporal sequence of PAD extracted from radar images for May 24th - 25th, 2011. Grey areas mark instant where a posteriori visual inspection confirmed the presence of the plume at Grimsvotn.*

Ash radar estimates. To derive quantitative results from the radar data we applied the Volcanic Ash Radar Retrieval for dual-Polarization X band systems (VARR-PX) (*Marzano et al., 2012*). The VARR aims at providing an automatic ash categorization and ash estimation making use of a synthetic dataset of the radar variables generated by a physical-electromagnetic forward model. The synthetic dataset allows building relationships between radar variables and physical parameters like ash concentration and ash fallout. The generation of the synthetic dataset is obtained by letting the ash particle size distribution parameters and the particle orientation, supposed to be spheroids, to vary in a random way. Additional information like ash particle density, axis ratio, dielectric constant are set up following values listed in table II in *Marzano et al, 2012*. Automatic discrimination of ash classes with respect to size (fine, coarse, small and lapilli, respectively FA, CA, SL and LL) implies the capability of classifying the radar volume reflectivity measurements into one of the four mentioned classes. Once the ash class is discriminated, then the ash concentration and fallout can be estimated by statistical techniques using the training simulated data sets. Within the VARR technique, the ash classification is performed by the use of maximum *a posteriori* (MAP probability) estimation. The probability density function (pdf) of each ash class (c), conditioned to the measured radar variables $\boldsymbol{x}_m$ is formulated using the Bayes theorem. The MAP estimation of ash class c corresponds to the maximization with respect to c of the posterior pdf $p(c|\,\boldsymbol{x}_m)$ under the assumption of multivariate Gaussian pdfs. The input radar variables that we used in this work for the VARR-PX algorithm for X-band radar, are the polarimetric measurements Z_{HH}, K_{DP} and ρ_{HV}. VARR-PX in its general configuration, consists of two main steps: i) classification of radar echoes with respect to ash particle size (in mm) (fine ash: FA, with average diameters of 0.01 mm; coarse ash: CA with average diameters of 0.1 mm; small lapilli: SL, with average diameters of 1 mm; large lapilli: LL, with average diameters of 10 mm) and orientation (prolate: PO, oblate: OO, and tumbling: TO); ii) estimation of the mass concentration C_a (in g/m^3) applying a suitable parametric power law (i.e. $C_a=a\bullet Z_{HH}{}^b$) with estimation parameters (i.e., a, b) varying according to the results of the previous classification step. For the Grímsvötn case study, Z_{DR} is not considered due to its calibration problems for DPX. For this reason the discrimination of the particle orientation, as foreseen in the full version of VARR-PX using Z_{DR}, is not performed since it would be not completely reliable. Additionally, the estimate of C_a, after the classification step, is performed considering only Z_{HH} because its use produces more robust and reliable results. Note that, even though we estimate the ash concentration for each radar bin using $C_a=a\bullet Z_{HH}{}^b$, the coefficients "a" and "b" depend on the predominant ash particle category at the considered grid point. This means that "a" and "b" depend from Z_{HH}, K_{DP} and ρ_{HV} which are used as input of the ash category classification scheme.

5 Results

The output of VARR-PX is shown in ***Figure 6*** where the vertical profiles of the predominant ash particle category (right panel) and ash concentration, C_a, (left panel), are shown. Looking at the ash categories, a transition between LL and FA is noted moving from the plume core (distance = 70 km) far away toward the radar site (distance =0 km). Some FA is also noted at the flanks of the plume and above height of 16 km. Within the core of the volcanic plume LL seems to coexist with SL particles. The mass concentration C_a (left panel) is higher on the left flank closer to the radar, than within its core. This behaviour seems to be consistent with the SSMIS images in figure 3 where the BT_H depression is more shifted toward the radar site than toward the Grímsvötn caldera. This is an encouraging result on the consistency of the VARR-PX approach. Note that the comparison of the vertical profiles of C_a (figure 6, left), and those of Z_{HH} (figure 1, upper left), may suggest an unphysical behaviour of C_a, that is, high values of reflectivity Z_{HH} above the volcano vent have correspond to lowest values of C_a and viceversa. Note that we used $C_a = aZ_{HH}{}^b$ and under the Rayleigh hypothesis Z_{HH} is proportional to the six moment of the particle size distribution so that Z_{HH} is more sensitive to particle diameter than C_a. This means that the consistency of Z_{HH} profiles should be compared with class of diameters (figure 6 right panel) more than ash concentration. Thus it may happen that the direct visual inspection between Z_{HH} and C_a estimates is not characterized by a high correlation. Noting at the distribution of ash class diameters (right panel of figure 6), the presence of LL below 8 km of altitude, as it results when using Z_{HH} K_{DP} and ρ_{HV} for classification, seems to be reasonable for the analysed eruption. When using only Z_{HH} we have a similar result without the presence of LL in the lower layers. In this respect, the added value of polarimetry, for the analysed case, is to make the VARR-PX output qualitatively more reliable. Quantitative experimental validations of radar retrievals would require an external reference within the ash cloud in proximity of the volcano vent, which is so far not available to our knowledge. Eventually, ***figure 7*** shows a quantitative comparison between SSMIS and DPX in terms of Total Columnar Concentration (*TCC*) of C_a. For the comparison of figure 6 we used the vertical cuts from DPX acquired 07:12 UTC on May 22nd 2011 at the azimuth of 21 deg from the North. To allow a better evaluation of the results, *TCCs* are averaged on the same reference grid of SSMIS to match its coarser grid resolution. The SSMIS channel used for the comparison is that at 183 ± 6 GHz. To convert BT_H [K] into *TCC* [kg/m^2] an inverse linear relation is applied $TCC=c_1+c_2BT_H(183\pm6)$ where c_1, c_2 are the empirically-based regression coefficients which are independent of the surface background and the atmospheric scene. The value of these coefficients is c_2=-1.062 and c_1=262.1 for DPX. The correlation of the SSMIS BT_H at 183 ± 6 GHz and *TCC* DPX radar retrieval has been found to be -0.67.

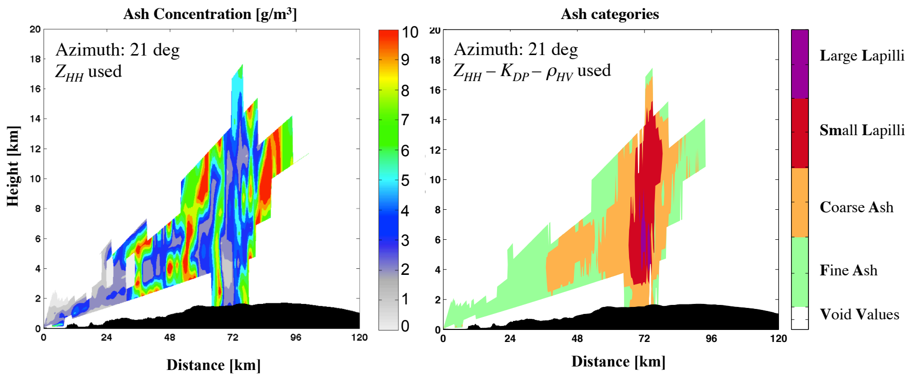

Figure 6*: VARR-PX outputs from RHI of radar data. Lef:, ash concentration. Right: ash categories.*

6 Conclusions

In this work ground polarimetric radar and satellite radiometer observations at microwave frequencies are exploited for the study of volcanic eruptions. The main conclusions for the analyzed case are: i) radar acquisition at X band can clearly detect the volcanic plume and the cloud spreading in the surrounding area of the Grímsvötn; ii) Since the low data quality, mainly due to the emergency circumstances of the Grímsvötn event, dual-polarization signatures from X band radar data, DPX, are not easy to interpret. The co-polar reflectivity Z_{HH} shows values greater than 25 dBZ within the plume core and values around 15 dBZ away from it. The correlation coefficient ρ_{HV} shows an abrupt decrease in the area interested by the core of the volcanic plume. This might be interpreted as a consequence of turbulent effects that facilitate the shuffling of various ash particles causing the decrease of ρ_{HV}. The differential reflectivity Z_{DR}, more than other radar variables, can be affected by factors depending from the radar system (bias) and the observed phenomena (depolarization induced by lightning and/or strong turbulences). This makes its interpretation challenging. Its behavior for the Grímsvötn case study seems to suggest non-spherical particles at the side of the plume as well as at lower elevations far from the core of the volcanic plume. Within the core of the volcanic plume, lower values of Z_{DR} are registered, suggesting tumbling or spherical particles; the specific differential phase K_{DP} shows positive increments within the plume. Additionally, the use of polarimetric variables has shown to provide more reliable qualitative results in terms of ash categories provided by VARR-PX output even though the differences of the columnar contents are minimal when compared with the use of Z_{HH} only. iii) the comparison of the total columnar concentration from DPX and brightness temperature at horizontal polarization, BT_H, from the satellite SSMIS radiometer, shows high correlation. This encourages the use of satellite microwave radiometers for ash estimation in the surrounding of the volcano vent, iv) The ash detection module here introduced is surely an useful tool in operational contexts especially for early warnings of upcoming eruptions even though its performance needs improvements for ash-meteo discrimination.

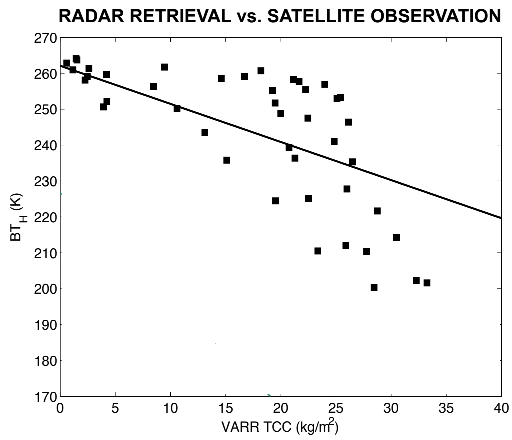

Figure 7*: Panel brightness temperature at horizontal polarization (BT_H) [K] from SSMIS versus the Total Columnar Content (TCC) [kg/m^2]. TCC is estimated through the VARR-PX technique using X-band Dual Polarization (DPX). DPX and SSMIS are acquired at 07:12 UTC and 07:15 UTC, respectively on May 22nd 2011 at the Grímsvötn site.*

7 Acknowledgements

A special thank is due to the Italian Dept. of Civil Protection (Italy) and to the Iceland Meteorological Office (Iceland) and to the World Wide Lightning Location Network (http://wwlln.net), Thanks to the European Commission through the Marie Curie Fellowship Grant number: 273666 and through the FP7 project FUTUREVOLC “A (Grant agreement no: 308377).

8 References

Bech, J., B. Codina, J. Lorente, and D. Bebbington, 2003: The sensitivity of single polarization weather radar beam blockage correction to variability in the vertical refractivity gradient. J. Atmos. Oceanic Technol., 20, 845–855.

Kramer, H. J., 2002: Observation of the Earth and Its Environment: Survey of Missions and Sensors, 4th edition, Springer, ISBN 3-540-42388-5.

Marzano F.S., Picciotti E., Vulpiani G., Montopoli M., 2012: Synthetic Signatures of Volcanic Ash Cloud Particles From X-Band Dual-Polarization Radar. IEEE Trans. Geosci. Rem. Sens., 50; 193-211, ISSN: 0196-2892, doi: 10.1109/TGRS.2011.2159225.

Montopoli M., Cimini D., Lamantea M., Herzog M., Graf H.F., and Marzano F.S. (2013),"Microwave radiometric remote sensing of volcanic ash clouds from space: model and data analysis", IEEE Transactions on Geoscience and Remote Sensing, vol. 51, (9), pp. 4678 – 4691, doi: 10.1109/TGRS.2013.2260343

Montopoli, M., Vulpiani, G., Cimini, D., Picciotti, E., Marzano, F.S.,” Interpretation of observed microwave signatures from ground dual polarization radar and space multi-frequency radiometer for the 2011 Grímsvötn volcanic eruption (2014) Atmospheric Measurement Techniques, 7 (2), pp. 537-552. doi: 10.5194/amt-7-537-2014.

Marzano, F. S., E. Picciotti, M. Montopoli, G. Vulpiani, 2013: Inside Volcanic Clouds: Remote Sensing of Ash Plumes Using Microwave Weather Radars. Bull. Amer. Meteor. Soc., 94, 1567–1586. doi: http://dx.doi.org/10.1175/BAMS-D-11-00160.1

Maki M., Maesaka T., Kozono T., Nagai M., Furukawa R., Nakada S., Koshida T., Takenaka H., 2012, Quantitative volcanic ash estimation by operational polarimetric weather radar, Proceedings of the 9th International Symposium on Tropospheric Profiling, L'Aquila, Italy, September 2012, ISBN: 978-90-815839-4-7.

Mastin, L.G., Guffanti, Marianne, Ewert, J.E., and Spiegel, Jessica, 2009: Preliminary spreadsheet of eruption source parameters for volcanoes of the world: U.S. Geological Survey Open-File Report 2009-1133, v. 1.2, 25 p. [http://pubs.usgs.gov/of/2009/1133/].

Petersen, G. N., Bjornsson, H., Arason, P. and Von Löwis , S., 2012: Two weather radar time series of the altitude of the volcanic plume during the May 2011 eruption of Grímsvötn, Iceland, Earth Syst. Sci. Data, 4, 121–127.

Rose, W. I., G. J. S. Bluth, and G. G. J. Ernst, 2000: Integrating retrievals of volcanic cloud characteristics from satellite remote sensors—A summary. Phil. Trans. R. Soc. A, 358, 1770, 1585–1606.

Ryzhkov A.V., Zrnic` D.S., 2007: Depolarization in Ice Crystals and Its Effect on Radar Polarimetric Measurements, J. Atm. Ocean. Tech., vol. 24, pp. 1256 – 1267, DOI: 10.1175/JTECH2034.1.

Ryzhkov A., 2007: The Impact of Beam Broadening on the Quality of Radar Polarimetric Data, Vol. 24, J. Atm. Ocean. Tech., DOI: 10.1175/JTECH2003.1

Vulpiani, G., M. Montopoli, L. Delli Passeri, A. Gioia, P. Giordano, F.S. Marzano, 2012: On the Use of Dual-Polarized C-Band Radar for Operational Rainfall Retrieval in Mountainous Areas. J. Appl. Meteor. Climatol., 51, 405–425.

Vulpiani, G., M. Montopoli, E. Picciotti , F.S. Marzano, 2011: On the use of polarimetric X-band weather radar for volcanic ash clouds monitoring, AMS Radar Conference, Pittsburgh (PA—USA).